IEEE Open Journal of the
Industrial Electronics Society

Received 25 December 2023; accepted 21 January 2024. Date of publication 12 February 2024;
date of current version 28 February 2024. The review of this article was arranged by Associate Editor Binbin Li.

Digital Object Identifier 10.1109/OJIES.2024.3361167

Power Imbalance Analysis of Modular Multilevel Converter With Distributed Energy Systems

TOMAS SALVADORES (Student Member, IEEE), JAVIER PEREDA (Senior Member, IEEE), AND FÉLIX ROJAS (Member, IEEE)

Department of Electrical Engineering and UC Energy Research Center, Pontificia Universidad Católica de Chile, Santiago 7820436, Chile

CORRESPONDING AUTHOR: JAVIER PEREDA (e-mail: jepereda@uc.cl)

This work was supported by the ANID under Grant 1220928 and Grant ANID/FONDAP/1523A0006, SERC Chile.

ABSTRACT The modular multilevel converter (MMC) can integrate distributed energy systems (DES), such as a battery energy storage system, to expand its functionalities and carry out multiple simultaneous tasks. However, a DES induces power imbalances within the MMC, which affects the operating currents and voltages of the converter. This phenomenon has been partially covered in recent works, but an analytical analysis has not yet been carried out to see the behavior and implications in different MMC-DES applications. This article introduces a novel analytical analysis of the power imbalances between MMC clusters. It pioneers the development of general equations and imbalance capability metrics, enabling the assessment of maximum currents and voltages supported by the MMC clusters. The developed tools allow the evaluation of any MMC-DES application regarding the current and voltage rating requirements of MMC clusters. The analysis shows that the MMC operating mode can substantially restrain or enlarge its imbalance capacity, affecting its suitability for different DES applications. While it needs around 33% current overrating in the worst imbalances, under some operating modes it can reach most imbalances without requiring current overrating. The ac compensation mode is much more capable of achieving imbalances than the dc compensation mode, reaching 88.37% and 16.74% of the imbalance points, respectively, without requiring any overrating.

INDEX TERMS Ac–dc power converters, modular multilevel converter (MMC), power imbalance, battery energy storage system (BESS), current rating, operation limit.

I. INTRODUCTION

The modular multilevel converter (MMC), also known as double star bridge cell, has gained much relevance during the last 20 years. Its modularity makes it convenient for medium to high voltage use cases and easy to maintain and repair. Although it is currently used in fields, such as high-voltage dc transmission and medium voltage motor drives, researchers continuously explore new applications to exploit its potential fully.

Several proposals exploit the fact the MMC can perform three conversion stages simultaneously by attaching a distributed energy system (DES) to the submodules (SMs), forming an MMC-DES (see Fig. 1). The SM dc-link capacitor, which is usually floating, can be connected to a DES component either directly or through a dc–dc conversion stage. An MMC-DES has the capacity to exchange energy in any direction between the two main ports and the DES, being able to carry out multiple simultaneous tasks.

The most widely proposed and studied type of DES is the distributed battery energy storage system (BESS) [1], [2], [3], [4]. Note that a BESS could also be used along an MMC in a centralized manner, by connecting it to the main dc-link, instead of as a DES. However, integrating the BESS in a distributed manner results in greater reliability and robustness to failures [3], [5]; is more efficient [6]; and reduces the dedicated battery management system hardware, as the state of charge (SoC) control can be performed actively by the MMC up to the SM level.

An MMC-BESS can interface ac and dc grids while providing complementary services [7], [8], [9], [10], which

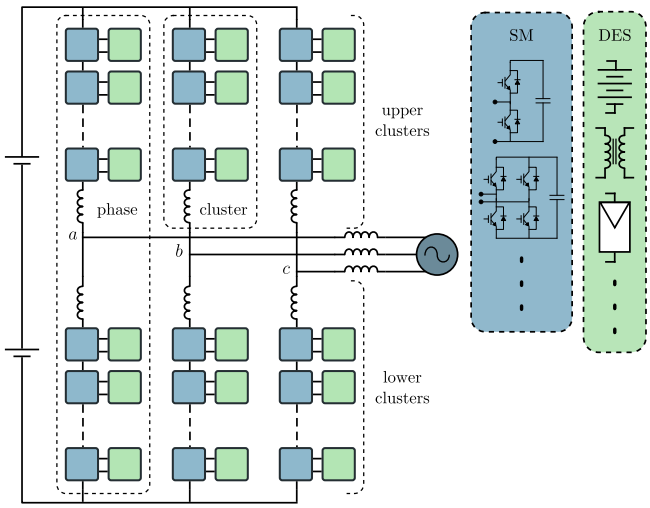

FIGURE 1. **MMC-DES topology.**

incorporates a new feature into a common MMC application. The MMC-BESS has also been studied to function as a STATCOM with active and reactive power provision [11], [12]. It can also be used to counter variability in wind generation at the turbine level, providing fault ride-through capability [13], or serve as the primary EV power conversion system [14], [15], [16], which are new fields for the MMC. One possible new application for the MMC-BESS is the implementation of second-life battery packs. As recycled batteries can vary greatly in their capacities, states of health (SoH) and remaining lifetime, the modularity in MMC-BESS control can be used to independently manage small subpackages of batteries depending on their specific requirements. In addition, the hardware modularity of the converter can be used to easily replace subpackages of batteries when they reach the end of their lifetimes without affecting the overall package.

Another studied DES is the distributed photovoltaic (PV) system [17], [18], which can manage a solar plant with a single converter while having great granularity in the maximum power point tracking (MPPT) control of different sections of the plant. Other proposed types of DES include solid-state transformers [19], [20], [21], [22] and hybrid DES [23], [24]. In particular, the hybrid MMC-PV-BESS has been recognized as a possible future trend [10], [25], [26].

Due to its distributed nature, a DES may transfer an uneven amount of power among the SMs, generating power imbalances within the converter. These imbalances can be large or small depending on the application, but all MMC-DES applications can be subjected to imbalances as a balanced DES can have an SM failure, affecting the power transfer of one SM. MMC-BESSs need to generate power imbalances to control the batteries SoC, which can be quite large if the batteries have poor SoH or if they are second-life heterogeneous batteries. Likewise, MMC-PVs require imbalances to handle the MPPT, which can be large under partial shading conditions.

MMC internal power imbalances can be classified into intracluster and intercluster. Intracluster imbalances occur among SMs within a single cluster, whose aggregated power is referred to as cluster power. Those imbalances can be managed through sorting of SMs [7], [27], [28] or by adjustments in their modulating voltages [2], [3], [29]. Intercluster imbalances occur between different clusters of the MMC and can be further subdivided into horizontal and vertical imbalances [30]. *Horizontal* refers to an imbalance between the aggregated power of different phases, while *vertical* refers to imbalances between the two clusters of the same phase. Intercluster imbalances are managed through circulating currents that distribute the power among the clusters without affecting the main MMC ports power [30], [31].

The minimal amount of circulating current occurs when all the power is evenly balanced among the clusters, whereas an unbalanced power distribution requires the injection of additional currents. Depending on the operating point, the new aggregated cluster currents can be higher or lower than the nominal currents, and they can grow considerably with large imbalances. Therefore, it is essential to determine the size of these currents during the design stage of the converter to select electrical components that can withstand them.

Analytical research on the effects of intercluster imbalances has been conducted on the cascaded H-bridge (CHB) [32], [33], but to the best of our knowledge, the MMC has not been studied from this approach. Existing work on MMC-DES intercluster imbalances conducts only numerical analysis and simulations for a bounded operating point and a specific application [7]. This approach lacks the generality that an analytical expression provides for both the converter operating point and type of DES. Former analytical research on the MMC-DES encompasses only intracluster imbalances [27], [34], [35], but considering only those imbalances limits the scope to SM voltage and DES current, leaving out cluster currents and voltages.

This article introduces a novel analytical analysis of the intercluster imbalances in an MMC, which has not been done before. Thus, the contribution of this article is in the development of general equations and new imbalance capability metrics that allow evaluating the maximum currents and voltages imposed to the MMC clusters. The developed analytical expressions are relevant as, to the best of our knowledge, currently there is no analytical formula to calculate the cluster current of an unbalanced MMC. The conducted analysis provides an in depth understanding of the effects that intercluster power imbalances have on the MMC. This article also proposes a mathematical representation of DESs based on their expected imbalance capabilities, and utilizes the new expressions to analyze the strain that different applications could exert on an MMC. The developed expressions were validated through experiments and simulations.

The rest of this article is organized as follows. Section II presents the MMC equations and the MMC-DES operating modes. Section III briefly describes the implemented control

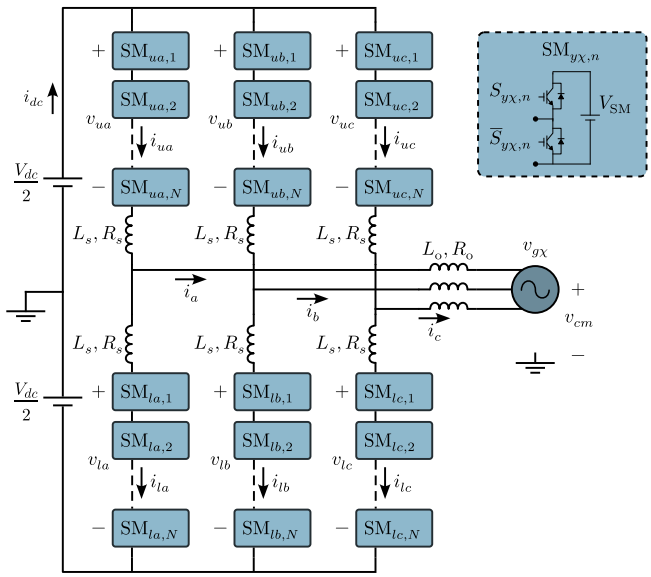

FIGURE 2. MMC-side model.

method. Section IV defines the imbalance metrics and derives the mathematical relation between converter variables and intercluster power imbalances. Section V analyzes how different possible MMC-DES imbalance ranges relate to the hardware overrating requirements. Section VI showcases the experimental and simulated results that validate the previous mathematical derivation and analysis. Finally, Section VII concludes this article.

II. CONVERTER MODEL

This work focuses on modeling the MMC-side of the MMC-DES, as it primarily concerns MMC design and analysis. From the perspective of the MMC-side, the DES-side can be seen as either a dc voltage source or a variable current source in the SMs. In this research, the DES is modeled as voltage sources because it facilitates the analysis and is more akin to the BESS application. Furthermore, the DES-side modeling depends on the DES type and is beyond the scope of this work.

A. MMC-SIDE MODEL

The MMC-side circuit model is illustrated in Fig. 2. The subscript $\chi \in \{a, b, c\}$ represents the phases, while $y \in \{u, l\}$ represents the upper or lower cluster per phase. Each submodule $\mathrm{SM}_{y\chi,n}$, $n \in \{1 \ldots N\}$, contains a capacitor whose voltage $v_{Cy\chi,n}$ sets the voltage available from the SM and is controlled to match the reference V_{SM}.

The voltage of all the connected SMs in one cluster adds up to form the cluster voltage $v_{y\chi}$. The converter model can be simplified by representing all the cluster SMs as an aggregated voltage source of value $v_{y\chi}$. While the cluster voltage is a switched voltage, the present modeling considers it to be equal to the modulated reference voltage, discarding the high-frequency components that relate to the switching. That approach is sufficient to analyze and control intercluster phenomenons, which are the concern of this work. Nevertheless, the switched model is still necessary to maintain a stable control of the intracluster phenomenons of the converter. Three groups of currents can be directly identified in the converter: the dc port current i_{dc}; the ac port currents i_χ; and the cluster currents $i_{y\chi}$. The cluster currents can be decoupled into two overlapping current sets, the circulating currents $i_{z\chi}$ that do not contribute to the output ac ports, and the currents that flow across the clusters into the ac port forming i_χ. The MMC currents are related by the following equations:

$$\begin{bmatrix} i_\chi \\ i_{z\chi} \end{bmatrix} = \begin{bmatrix} 1 & -1 \\ 1/2 & 1/2 \end{bmatrix} \cdot \begin{bmatrix} i_{ux} \\ i_{lx} \end{bmatrix} \tag{1}$$

$$i_{\mathrm{dc}} = \sum_\chi i_{z\chi}. \tag{2}$$

All converter currents can be defined by only i_χ and $i_{z\chi}$ (1), (2). Both their state equations can be derived from the Kirchoff's voltage law and (1), but they have coupled control variables $v_{u\chi}$ and $v_{y\chi}$. This can be overcome by defining and applying a $\Sigma\Delta$ transform [36] [37] to the cluster voltages

$$\begin{bmatrix} v_\chi^\Sigma \\ v_\chi^\Delta \end{bmatrix} = \frac{1}{2} \begin{bmatrix} 1 & 1 \\ -1 & 1 \end{bmatrix} \cdot \begin{bmatrix} v_{u\chi} \\ v_{l\chi} \end{bmatrix}. \tag{3}$$

It is noted that the common mode voltage of the converter is directly related to the zero sequence component of v_χ^Δ as

$$v_{\mathrm{cm}} = \sum_\chi \frac{v_{l\chi} - v_{u\chi}}{6} = \sum_\chi \frac{v_\chi^{\Delta+} + v_\chi^{\Delta-} + v^{\Delta 0}}{3} = v^{\Delta 0}. \tag{4}$$

Two auxiliary terms are defined to write the state equations in a more compact manner

$$R_\epsilon = \frac{R_s + 2R_o}{2}, \quad L_\epsilon = \frac{L_s + 2L_o}{2}. \tag{5}$$

Replacing (3), (4), and (5) in the standard state equations yields the final state equations

$$\frac{di_\chi}{dt} = \frac{1}{L_\epsilon}\left(v_\chi^{\Delta+-} - R_\epsilon i_\chi - v_{g\chi}\right) \tag{6}$$

$$\frac{di_{z\chi}}{dt} = \frac{1}{L_s}\left(-v_\chi^\Sigma - R_s i_{z\chi} + \frac{V_{\mathrm{dc}}}{2}\right). \tag{7}$$

The MMC power analysis is typically summarized into the ac and dc ports power

$$P_{\mathrm{ac}} = -\frac{3I_g V_g}{2}, \quad P_{\mathrm{dc}} = I_{\mathrm{dc}} V_{\mathrm{dc}}. \tag{8}$$

The negative and positive signs of the ac and dc powers are due to the direction of the currents defined in Fig. 2.

In presence of a DES, it is essential to also consider the cluster power $P_{y\chi}$ in the analysis of the converter. The cluster power is the power that each cluster sends or receives from the DES. For convenience, the $\Sigma\Delta$ transform is applied to the cluster powers as well, obtaining P_χ^Σ and P_χ^Δ. The original

cluster powers are just

$$P_{u\chi} = P_{\chi}^{\Sigma} - P_{\chi}^{\Delta}, \quad P_{l\chi} = P_{\chi}^{\Sigma} + P_{\chi}^{\Delta} \tag{9}$$

where P_{χ}^{Σ} is the average cluster power of phase χ, and P_{χ}^{Δ} is the power imbalance between the clusters of phase χ.

Due to the principle of orthogonality of different frequencies h, the clusters power can be desegregated into each frequency contribution

$$P_{\chi}^{\Sigma\Delta} = \sum_{h} P_{\chi,h}^{\Sigma\Delta} \tag{10}$$

where in this case $h \in \{0, 1\}$. The power equations can be derived by better defining the converter variables

$$\begin{aligned} v_{g\chi} &= V_g \sin(\omega t + \theta_{\chi}) \\ i_{\chi} &= I_g \sin(\omega t + \theta_{\chi}) \\ i_{z\chi,0} &= I_{z\chi,0} \\ i_{z\chi,1} &= I_{z\chi,1} \sin(\omega t + \phi_{z\chi}) \end{aligned} \tag{11}$$

where θ_{χ} is the grid voltage phase angle and $\phi_{z\chi}$ is the angle of the circulating current respect to the phase angle. The converter is assumed to operate with unitary power factor, and thus it is assumed that the i_{χ} current is controlled to match the θ_{χ} grid voltage angle. Setting aside the active power oscillating components, the resultant equations are the following:

$$P_{\chi,0}^{\Sigma} = -R_s {I_{z\chi,0}}^2 + \frac{1}{2} V_{\mathrm{dc}} I_{z\chi,0} \tag{12}$$

$$P_{\chi,0}^{\Delta} = 0 \tag{13}$$

$$P_{\chi,1}^{\Sigma} = -\frac{1}{2} R_s \left({I_{z\chi,1}}^2 + \frac{{I_g}^2}{4} \right) - \frac{1}{4} R_o I_g^2 - \frac{1}{4} V_g I_g \tag{14}$$

$$\begin{aligned} P_{\chi,1}^{\Delta} = \frac{1}{2} I_{z\chi,1} [&(R_s + R_o) I_g \cos(\phi_{z\chi} - \theta_{\chi}) \\ &+ \omega L_o I_g \sin(\phi_{z\chi} - \theta_{\chi}) + V_g \cos(\phi_{z\chi} - \theta_{\chi})]. \end{aligned} \tag{15}$$

B. OPERATING MODES

All powers are considered positive when entering the converter and negative when leaving the converter

$$P_{\mathrm{dc}} + P_{\mathrm{ac}} + P_{\mathrm{des}} = 0 \tag{16}$$

$$P_{\mathrm{des},y\chi} = -P_{y\chi}. \tag{17}$$

The integration of DES power into the MMC power flow is modeled by defining two categories, dc compensation and ac compensation. Dc compensation is when the net changes in DES power are corresponded with changes in the dc port power, with independent power control of the ac port. Conversely, ac compensation is when the net changes in DES power are corresponded with changes in the ac port power, with independent power in the dc port. This work revolves around the limitations of the MMC-DES operation, so the independent port is considered to be at nominal power.

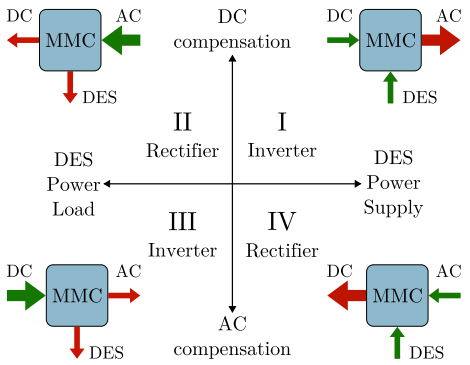

FIGURE 3. Operating modes diagram.

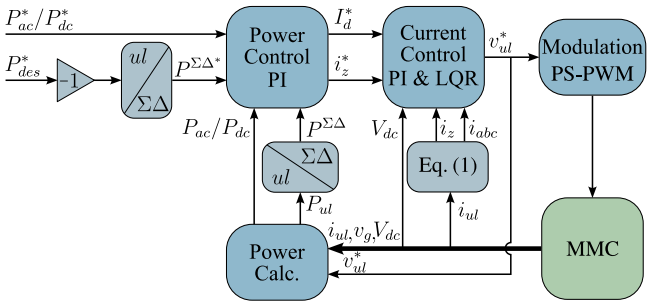

FIGURE 4. Implemented MMC-side control of the MMC-DES.

It is set that the main ports cannot exceed its nominal power value, rendering some operating modes unfeasible. For example, if the ac port is fixed at its nominal value acting as an inverter, a negative DES power value would make the dc port contribute more than its nominal value, which is considered unfeasible. This condition yields the four operating modes illustrated in Fig. 3.

III. CONTROL IMPLEMENTATION

To integrate the control of an MMC and a DES, one of them must control the SM capacitor voltage, while the other controls the flow of current and hence the power. Either side can perform each task, but depending on the application, usually one way is more convenient than the other. In this article, the DES is selected to control the capacitor voltage, which allows to model it as a fixed voltage source and focus into the MMC-side control. Furthermore, the DES-side control depends on the DES at issue and is out of the scope of this work.

The implemented MMC-side control (see Fig. 4) encompasses only the essential control objectives for stable converter operation, aiming to study the MMC from the most possible general perspective. The authors in [24] provided alternative dc/ac compensation controls, with more detail. Other important references for MMC-DES control but that do not make distinction between compensations are [3], [31], and [30].

A. POWER CONTROL

Only two powers are controlled and the third forcefully changes its value bounded by the expression (16). To ensure proper control over the DES constituents, the DES power must always be controlled. The second controlled power depends on the type of compensation. The compensated port must adjust its value dynamically depending on the changes in the DES power. Meanwhile, the uncompensated or fixed port must maintain its value independently of the DES contribution. The approach that best fits the described behavior, is to control the fixed port and to leave the compensated port subject to the others.

1) IMBALANCE CONTROL

Σ power can be used to manage horizontal imbalances, and Δ power can be used to manage vertical imbalances. Discarding the losses, (12) and (14) show that only the dc circulating currents and the ac grid current contribute Σ power, and thus affect horizontal balance. Equations (13) and (15) show that the ac circulating current is the only current that significantly contributes Δ power, thus affecting vertical balance.

2) DC COMPENSATION

The dc compensation control is designed to receive references for the ac port power and the DES power. The ac port control generates output ac current references. The DES control generates ac circulating current references and dc circulating current references that add up to the dc port current, as shown in (2). Thus, the DES power control indirectly controls the dc port power.

3) AC COMPENSATION

The ac compensation control is designed to receive references for the dc port power and the DES power. The dc port control generates the reference for the sum of all dc circulating currents. The DES control generates ac circulating current references and the ac output current reference. Thus, the DES power control indirectly controls the ac port power. In this case, the DES control generates dc circulating current components that add up with the dc port control currents, to manage the horizontal imbalances.

B. COMPENSATORY CURRENTS

The use of ac circulating current for vertical imbalances entails an issue. If an imbalance is required in one of the phases and not in the others, the ac current that will flow into the converter must come from the dc link to close the path for the current. To solve this issue, Munch et al. [30] proposed the use of compensatory currents $i^c_{z\chi}$. When an imbalance is required in one phase, these currents are injected into the other phases with an angle such that they do not produce active power, and with a magnitude such that they balance the power-producing (or primary) current $i^p_{z\chi}$. This mechanism is described by Fig. 5 and the following equations:

$$i_{z\chi,1} = i^p_{z\chi} + i^c_{z\chi} \tag{18}$$

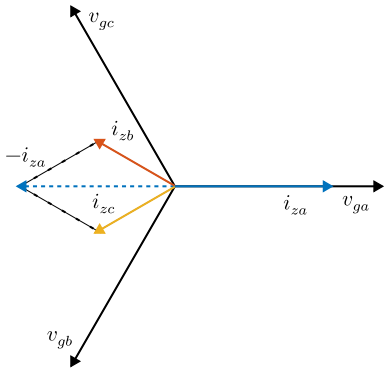

FIGURE 5. Compensatory currents. Vertical imbalance only in phase *a*.

$$i^p_{z\chi} = I^p_{z\chi}\cos(\omega t + \theta_\chi) \tag{19}$$

$$i^c_{z\chi} = I^c_{z\chi}\cos(\omega t + \theta_\chi + 90^\circ) \tag{20}$$

$$I^c_{z\chi} = \begin{cases} \frac{1}{\sqrt{3}}(I^p_{zb} - I^p_{zc}), & \chi = a \\ \frac{1}{\sqrt{3}}(I^p_{zc} - I^p_{za}), & \chi = b \\ \frac{1}{\sqrt{3}}(I^p_{za} - I^p_{zb}), & \chi = c. \end{cases} \tag{21}$$

IV. IMBALANCE MODEL

The aim of the forthcoming mathematical derivation is to find equations that can express the changes in the maximum converter current and voltage as a function of the intercluster power imbalance of the MMC. In order to do that, two new factors are defined: i) the intercluster imbalance factors λ; and ii) the overrating factors ζ for cluster voltage and current.

The imbalance factors λ^Σ_χ and λ^Δ_χ are the $\Sigma\Delta$ DES powers normalized by the power that they could achieve if the DES were to supply all the nominal power of one of the converter grid ports P^{nom}

$$\lambda^\Sigma_\chi = \frac{P^\Sigma_{\text{des},\chi}}{P^{\text{nom}}/6} \Longrightarrow P^\Sigma_{\text{des},\chi} = \frac{\lambda^\Sigma_\chi P^{\text{nom}}}{6} \tag{22}$$

$$\lambda^\Delta_\chi = \frac{P^\Delta_{\text{des},\chi}}{P^{\text{nom}}/6} \Longrightarrow P^\Delta_{\text{des},\chi} = \frac{\lambda^\Delta_\chi P^{\text{nom}}}{6}. \tag{23}$$

Note that for the hereby defined operating modes, the λ factors are restricted to operate within $[-1, 1]$. However, the factors could eventually operate outside that range and this derivation is also valid in that case.

The overrating factors $\zeta_{i\chi}$ and $\zeta_{v\chi}$ are the maximum value that the cluster current and voltage reach in a determined unbalanced state, divided by the maximum value of that variable in its nominal balanced state

$$\zeta_{i\chi}(\vec{\lambda}) = \frac{\max\limits_{y,t}\{|i_{y\chi}|\}}{I^{\text{nom}}_{y\chi}} \tag{24}$$

$$\zeta_{v\chi}(\vec{\lambda}) = \frac{\max\limits_{y,t}\left\{|v_{y\chi} - \frac{V_{\text{dc}}}{2}|\right\}}{\max\limits_{y,t}\left\{|v^{\text{nom}}_{y\chi} - \frac{V_{\text{dc}}}{2}|\right\}} \tag{25}$$

where $I_{y\chi}^{\text{nom}}$ is the maximum value of the cluster currents during nominal converter operation. It can be derived from the power equations (8) and relations (1)

$$I_{y\chi}^{\text{nom}} = \max_{y,t}\{|i_{y\chi}^{\text{nom}}|\} = \frac{P^{\text{nom}}}{3}\left(\frac{1}{V_{\text{dc}}} + \frac{1}{V_g}\right). \tag{26}$$

The overrating factors are calculated for both dc and ac compensation schemes, yielding $\zeta_{i\chi}^{\text{dc}}$, $\zeta_{i\chi}^{\text{ac}}$, $\zeta_{v\chi}^{\text{dc}}$, and $\zeta_{v\chi}^{\text{ac}}$.

The power direction between the converter grid ports is represented by a constant κ

$$\kappa = \begin{cases} 1: & \text{inverter} \\ -1: & \text{rectifier.} \end{cases} \tag{27}$$

A dc link overrating factor ζ_{dc} is also defined to enable cleaner analytic expressions

$$\zeta_{\text{dc}} = \frac{V_{\text{dc}}}{V_g}. \tag{28}$$

The next procedure drops the loss terms from the power equations, since even though it introduces an error, including them results in huge and utterly impractical expressions.

A. DC COMPENSATION

In dc compensation mode, the ac port power is always fixed at its nominal value, which means that

$$P_{\text{ac}} = -\kappa P^{\text{nom}}. \tag{29}$$

Then, it follows from (8) and (29) that under dc compensation:

$$I_g = \frac{2\kappa P^{\text{nom}}}{3V_g}. \tag{30}$$

1) CURRENT OVERRATING ($\zeta_{i\chi}^{dc}$)

All the overrating expressions are derived from the $\Sigma\Delta$ transform to the relation (17)

$$P_{\chi,0}^{\Sigma} + P_{\chi,1}^{\Sigma} = -P_{\text{des},\chi}^{\Sigma} \tag{31}$$

$$P_{\chi,1}^{\Delta} = -P_{\text{des},\chi}^{\Delta}. \tag{32}$$

The impact of horizontal imbalances on the converter currents can be derived from (22), (30), and (31) discarding the loss terms

$$I_{z\chi,0} = \frac{P^{\text{nom}}}{3\zeta_{\text{dc}}V_g}\left(\kappa - \lambda_{\chi}^{\Sigma}\right). \tag{33}$$

The impact of vertical imbalances on the converter currents can be derived from (32), (23), and discarding the loss terms

$$I_{z\chi,1}^{p} = -\frac{\lambda_{\chi}^{\Delta} P^{\text{nom}}}{3V_g}. \tag{34}$$

This term is only the primary component of the ac circulating currents. The primary current is by definition in phase with the phase voltage. The total ac circulating current of one phase depends also on the compensatory currents $i_{z\chi}^{c}$, as shown in Fig. 6. Therefore, ac circulating current

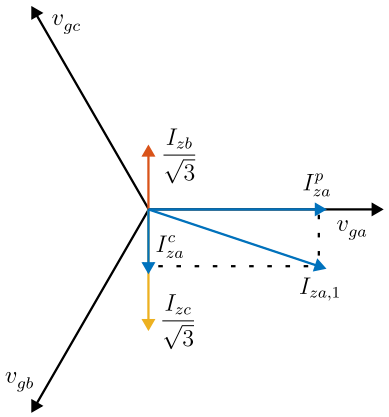

FIGURE 6. Magnitude of ac circulating current component.

magnitude is

$$I_{z\chi,1} = \frac{P^{\text{nom}}}{3V_g}\Gamma_{\chi}(\vec{\lambda^{\Delta}}) \tag{35}$$

where Γ_{χ} and the current phase are

$$\Gamma_{\chi}(\vec{\lambda^{\Delta}}) = \sqrt{{\lambda_{\chi}^{\Delta}}^2 + \frac{1}{3}\sum\nolimits_{j\neq\chi}{\lambda_j^{\Delta}}^2 - \frac{2}{3}\prod\nolimits_{j\neq\chi}\lambda_j^{\Delta}} \tag{36}$$

$$\phi_{z\chi}(\vec{\lambda^{\Delta}}) = \cos^{-1}\left(\frac{-\lambda_{\chi}^{\Delta}}{\Gamma_{\chi}}\right). \tag{37}$$

The ac cluster current magnitude is found through a trigonometric identity

$$|i_{y\chi,1}| = |i_{z\chi,1} \pm \frac{i_{\chi}}{2}| = \sqrt{{I_{z\chi,1}}^2 + \frac{{I_g}^2}{4} \mp I_{z\chi,1} I_g \frac{\lambda_{\chi}^{\Delta}}{\Gamma_{\chi}}}. \tag{38}$$

The maximum cluster current can be disaggregated into two components

$$\max_{y,t}\{|i_{y\chi}|\} = \max_{y,t}\{|i_{z\chi,0}|\} + \max_{y,t}\{i_{y\chi,1}\} \tag{39}$$

where from (33)

$$\max_{y,t}\{|i_{z\chi,0}|\} = \frac{P^{\text{nom}}}{3\zeta_{\text{dc}}V_g}\left|\kappa - \lambda_{\chi}^{\Sigma}\right| \tag{40}$$

and from (38)

$$\max_{y,t}\{i_{y\chi,1}\} = \frac{P^{\text{nom}}}{3V_g}\sqrt{{\Gamma_{\chi}}^2 + 2\left|\lambda_{\chi}^{\Delta}\right| + 1}. \tag{41}$$

Ultimately, the maximum current overrating of each phase is

$$\zeta_{i\chi}^{\text{dc}}(\vec{\lambda}) = \frac{\left|\kappa - \lambda_{\chi}^{\Sigma}\right| + \zeta_{\text{dc}}\sqrt{{\Gamma_{\chi}}^2 + 2\left|\lambda_{\chi}^{\Delta}\right| + 1}}{1 + \zeta_{\text{dc}}}. \tag{42}$$

2) VOLTAGE OVERRATING ($\zeta_{v\chi}^{dc}$)

The voltage overrating factor is found by replacing the current expressions in the steady state equations (6) and (7), applying a trigonometric identity, and simplifying the voltage phases to

the worst cases, resulting in

$$\zeta_{v\chi}^{\mathrm{dc}}(\vec{\lambda}) = \frac{\frac{P^{\mathrm{nom}}}{3V_g}\left(Z_s|\Gamma_\chi| + \frac{R_s}{\zeta_{\mathrm{dc}}}|\kappa - \lambda_\chi^\Sigma|\right) + V_1^\Delta}{\frac{R_s P^{\mathrm{nom}}}{3\zeta_{\mathrm{dc}} V_g} + V_1^\Delta} \tag{43}$$

where

$$V_1^\Delta = \sqrt{\left(\frac{2P^{\mathrm{nom}}Z_s}{3V_g}\right)^2 + \frac{4\kappa P^{\mathrm{nom}}R_\epsilon}{3} + {V_g}^2} \tag{44}$$

$$Z_s = \sqrt{\omega^2 L_s^2 + R_s^2}. \tag{45}$$

B. AC COMPENSATION

In ac compensation mode, the dc port power is always fixed at its nominal value, which means that

$$P_{\mathrm{dc}} = \kappa P^{\mathrm{nom}}. \tag{46}$$

The expressions (2), (8), and (46) imply that under ac compensation

$$\sum_\chi I_{z\chi,0} = \frac{\kappa P^{\mathrm{nom}}}{V_{\mathrm{dc}}}. \tag{47}$$

In (47), ac compensation mode establishes a condition for the sum of the dc circulating currents, whereas dc compensation established a condition for the currents themselves. Therefore, in this case is of practical use to define the following new auxiliary imbalance factors:

$$\lambda_{\mathrm{avg}}^\Sigma = \frac{1}{3}\sum_\chi \lambda_\chi^\Sigma \tag{48}$$

$$\lambda_{\delta\chi}^\Sigma = \lambda_\chi^\Sigma - \lambda_{\mathrm{avg}}^\Sigma. \tag{49}$$

1) CURRENT OVERRATING ($\zeta_{i\chi}^{ac}$)

From (17) is evident that

$$\sum_\chi \left(P_{\chi,0}^\Sigma + P_{\chi,1}^\Sigma\right) = \sum_\chi -P_{\mathrm{des},\chi}^\Sigma. \tag{50}$$

Evaluating (47) and (48) into (50), and discarding the loss terms yields

$$I_g = \frac{2P^{\mathrm{nom}}}{3V_g}\left(\kappa + \lambda_{\mathrm{avg}}^\Sigma\right) \tag{51}$$

and evaluating (51) in the relation (31) eventually yields

$$I_{z\chi,0} = \frac{P^{\mathrm{nom}}}{3\zeta_{\mathrm{dc}}V_g}\left(\kappa - \lambda_{\delta\chi}^\Sigma\right). \tag{52}$$

The $I_{z\chi,1}$ current is the same as previously. Following the same procedure as in dc compensation, the current overrating factor for a determined operating point is

$$\zeta_{i\chi}^{\mathrm{ac}}(\vec{\lambda}) = \frac{|\kappa - \lambda_{\delta\chi}^\Sigma| + \zeta_{\mathrm{dc}}\sqrt{{\Gamma_\chi}^2 + (\kappa + \lambda_{\mathrm{avg}}^\Sigma)^2 + 2\left|(\kappa + \lambda_{\mathrm{avg}}^\Sigma)\lambda_\chi^\Delta\right|}}{1 + \zeta_{\mathrm{dc}}}. \tag{53}$$

2) VOLTAGE OVERRATING ($\zeta_{v\chi}^{ac}$)

Following again the same procedure as in dc compensation, the voltage overrating is

$$\zeta_{v\chi}^{\mathrm{ac}}(\vec{\lambda}) = \frac{\frac{P^{\mathrm{nom}}}{3V_g}\left(Z_s|\Gamma_\chi| + \frac{R_s}{\zeta_{\mathrm{dc}}}|\kappa - \lambda_{\delta\chi}^\Sigma|\right) + V_1^\Delta(\vec{\lambda^\Sigma})}{\frac{R_s P^{\mathrm{nom}}}{3\zeta_{\mathrm{dc}}V_g} + V_1^\Delta(\vec{0})} \tag{54}$$

where

$$V_1^\Delta(\vec{\lambda^\Sigma}) = \sqrt{\left(\frac{2P^{\mathrm{nom}}Z_s}{3V_g}\right)^2 (\kappa + \lambda_{\mathrm{avg}}^\Sigma)^2 + \frac{4P^{\mathrm{nom}}R_\epsilon}{3}(\kappa + \lambda_{\mathrm{avg}}^\Sigma) + {V_g}^2}. \tag{55}$$

C. DISCUSSION

It is quite interesting to point out that both current overrating factors (42), (53) do not depend on any of the converter physical parameters. They only depend on the characteristics of the imbalance ($\lambda^{\vec{\Sigma\Delta}}$), the operating mode ($\kappa$ and compensation), and the proportion between the grid voltages (ζ_{dc}). This indicates that, in principle, the imbalance phenomenon behaves in the same manner in all MMCs (regarding currents). Nevertheless, losses do not, so the current expressions would incorporate converter parameters if the losses had been taken into consideration. On the other hand, the voltage overrating does depend on the converter parameters.

Another interesting finding arises by contrasting the found current overrating expressions (42), (53) and modes of operation defined in Fig. 3. For each quadrant of the diagram, the λ_χ^Σ terms and κ have always the same sign under dc compensation, and opposed signs under ac compensation. This means that at least any balanced participation of the DES on the power transfer decreases the cluster currents. The expressions show that horizontal imbalances can increase or decrease the converter currents, but any vertical imbalance will always produce an increase on the converter currents. Closer inspection reveals that, while pure horizontal imbalances can produce current increases, those increases cannot exceed converter nominal rating. Therefore, the overrating expressions demonstrate that the converter nominal current rating can only be exceeded in presence of vertical imbalances.

V. CONVERTER RATING ANALYSIS

An MMC-DES is expected to operate within a range of imbalances, rather than in a fixed imbalance. It is relevant to know in detail matters such as the maximum overrating that a converter may need to withstand over a range of different imbalances; the imbalances that a converter can reach for a given overrating; or what is the progressive tradeoff between overrating requirements and different kinds of imbalances.

In practical terms for MMC rating, a DES can be represented by all the imbalances it may impose on the joint system, which is referred to as the power imbalance space (PIS). The PIS can vary greatly depending on the application and implementation. This space is defined by boundaries for

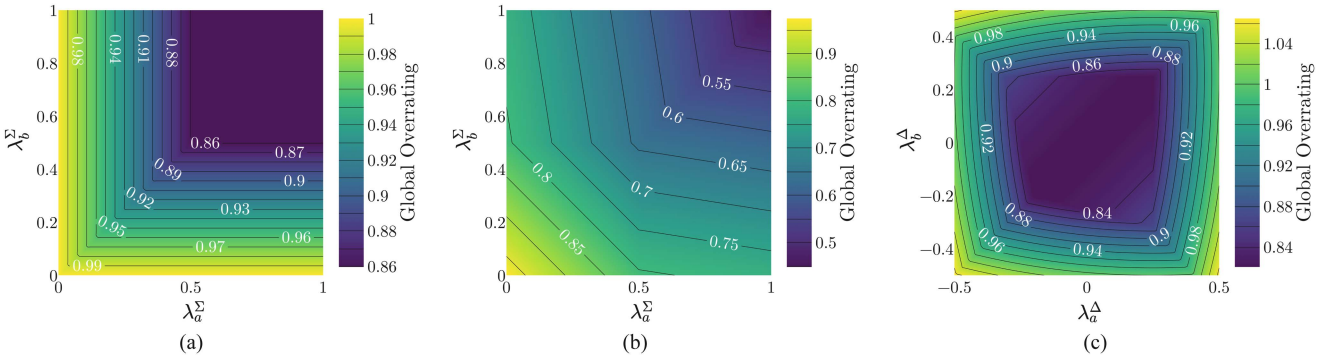

FIGURE 7. Effects of imbalances on current overrating. (a) Horizontal imbalances under dc compensation. $\lambda_c^{\Sigma} = 0.5$, $\lambda_{\chi}^{\Delta} = 0\ \forall\ \chi$. (b) Horizontal imbalances under ac compensation. $\lambda_c^{\Sigma} = 0.5$, $\lambda_{\chi}^{\Delta} = 0\ \forall\ \chi$. (a) Vertical imbalances under ac compensation. $\lambda_c^{\Delta} = 0.25$, $\lambda_{\chi}^{\Sigma} = 0.5\ \forall\ \chi$.

TABLE 1. General PISs

PIS	Boundaries	Constrains	Application example
Λ_1	$0 \le \lambda_{\chi}^{\Sigma} \le 1$ $-0.5 \le \lambda_{\chi}^{\Delta} \le 0.5$	$0 \le \lambda_{\chi}^{\Sigma} + \lambda_{\chi}^{\Delta} \le 1$ $0 \le \lambda_{\chi}^{\Sigma} - \lambda_{\chi}^{\Delta} \le 1$	PV or BESS under unbalanced discharging
Λ_2	$-1 \le \lambda_{\chi}^{\Sigma} \le 0$ $-0.5 \le \lambda_{\chi}^{\Delta} \le 0.5$	$-1 \le \lambda_{\chi}^{\Sigma} + \lambda_{\chi}^{\Delta} \le 0$ $-1 \le \lambda_{\chi}^{\Sigma} - \lambda_{\chi}^{\Delta} \le 0$	BESS under unbalanced charging

TABLE 2. Current Global Overrating for Λ_1

Compensation	Solution (worst op. point)	Overrating (ζ_i)
dc	$\vec{\lambda^{\Sigma}} = [0.5, 0.5, 0.5]^T$ $\vec{\lambda^{\Delta}} = [0.5, -0.5, -0.5]^T$	1.296 (clusters ub and uc)
ac	$\vec{\lambda^{\Sigma}} = [0, 0.5, 0]^T$ $\vec{\lambda^{\Delta}} = [0, -0.5, 0]^T$	1.333 (cluster lb)

the values of each λ term, and constrains that encompass the relations between $\vec{\lambda^{\Sigma}}$ and $\vec{\lambda^{\Delta}}$. Table I defines two general PISs that represent the broadest cases for fully rated DES imbalances, which serve to analyze the MMC-DES from a general perspective and evaluate the worst cases.

A. GLOBAL OVERRATING

The overrating factors can be fed into an optimization problem to find the global overrating required by the converter. The global overrating is the maximum overrating that will be needed in any cluster across all the defined Λ of a DES application

$$\begin{aligned} \zeta_i = \quad & \max_{\chi,\lambda} \left\{ \zeta_{i\chi}(\vec{\lambda}) \right\} \\ & \text{s.t.} \quad \chi \in \{a, b, c\} \\ & \qquad \lambda \in \Lambda. \end{aligned} \tag{56}$$

The $\zeta_{i\chi}$ expressions are symmetrical for Λ_1 and Λ_2 under the predefined operation modes. The ζ_i yields the same results in both PISs, but with opposed $\vec{\lambda^{\Sigma}}$ signs. The optimization yields six equivalent solutions for each compensation (see Table II). It shows that the most straining ζ_i^{dc} occurs with the maximum vertical imbalance in one direction on two phases and the maximum vertical imbalance in the opposite direction on the remaining phase. On the other hand, the most straining ζ_i^{ac} occurs when one phase is contributing half its nominal power with the maximum vertical imbalance, while the other phases contribute the minimum power. The most straining imbalances in ac compensation mode require more current overrating (33%) than in dc compensation mode (30%).

Calculating ζ_v shows that the required voltage overrating is relatively small, below 6% in all cases, which can be considered within the modulator slack margin. Therefore, MMC-DES overvoltages should not pose a big complication and will be omitted from the forthcoming analysis.

B. IMBALANCE EFFECTS ON OVERRATING

Under dc compensation, horizontal imbalances demand overrating solely in relation to the least power-exchanging phase [see Fig. 7(a)], regardless of the total DES power. Meanwhile, horizontal imbalances under ac compensation have a present but lesser effect, as the required overrating depends mostly on the total DES power [see Fig. 7(b)]. The ac compensated modes seem to demand less overrating overall, and the DES power distribution is much more impactful under dc compensation.

Vertical imbalances have the same effects on overrating under both compensations [see Fig. 7(c)], but dc compensation has a higher overrating baseline due to its different response to horizontal imbalances. They increasingly demand overrating in relation to the magnitude of the imbalances, but do a bit less so if all imbalances have the same sign. That occurs because if all the imbalances are of the same sign and magnitude, the currents that produce the vertical imbalances are balanced, and there is no compensatory current injection.

C. POWER IMBALANCE CAPABILITY OF THE MMC

A generic metric is defined to quantify the imbalance capability of power converters with DES integration, evaluate them, and compare them. This is the power imbalance factor (PIF),

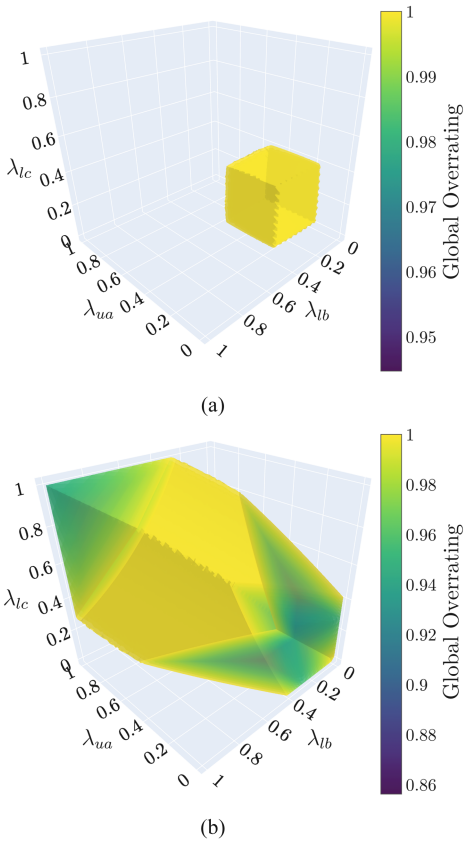

FIGURE 8. PIR 3-D slices. $\lambda_{y\chi} = 0.3$, $\forall y\chi \notin \{ua, lb, lc\}$. (a) Dc compensation. (a) Ac compensation.

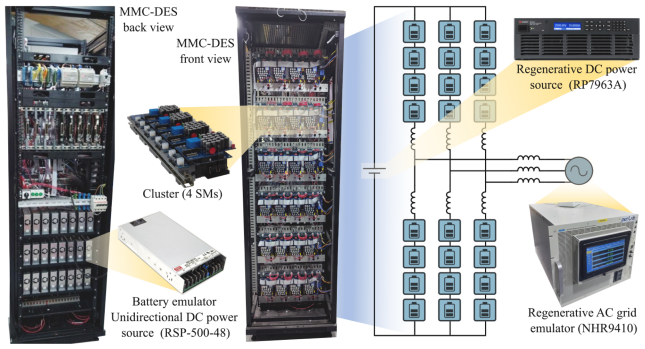

FIGURE 9. Experimental setup.

TABLE 3. Experiment Parameters

Description	Parameter	Value
Nominal power	P^{nom}	600 W
Dc grid voltage	V_{dc}	192 V
Ac grid voltage	V_g	75 V
Cluster inductance	L_s	5 mH
Output inductance	L_o	1 mH
Cluster resistance	R_s	0.96 Ω
Output resistance	R_o	0.31 Ω
SM dc source voltage	V_{SM}	48 V
SMs per cluster	N	4
Carrier frequency	f_{sw}	2.5 kHz

inspired on work from [33] on CHB-PV imbalances, but considering current and/or voltage restrictions. The consideration of a current or voltage restriction depends solely on their relevance. For example, current restrictions are not relevant for a CHB in Star configuration, because its currents are always below nominal under imbalances [33]. The optimization problem showed that overvoltages in MMC imbalances should be noted, but are not much of an issue. Therefore, the MMC PIF hereby only considers current bounds.

The PIF is calculated as the division between the volumes of the power imbalance region (PIR) and the PIS of the DES, resulting in a value within [0, 1]. The PIR is the multidimensional region within the PIS that is bounded by rating restrictions over the converter current and/or voltage. The PIR of the MMC cannot be fully visualized, as it is a 6-D region, but a 3-D slice can still provide a valuable sense of the feasibility of different imbalances in the MMC. Fig. 8 shows PIR slices with $\lambda_{y\chi}$ imbalance factors that represent individual cluster imbalances and are obtained from the former factors through the inverse $\Sigma\Delta$ transform.

The PIF of an MMC can be calculated as

$$\text{PIF} = \frac{\int \cdots \int_{\Lambda} Z(\vec{\lambda})\, d\Lambda}{\int \cdots \int_{\Lambda} 1\, d\Lambda} \tag{57}$$

where,

$$Z(\vec{\lambda}) = \begin{cases} 1, & \max\limits_{\chi} \left\{ \zeta_{i\chi}(\vec{\lambda}) \right\} \leq \zeta^{\max} \\ 0, & \max\limits_{\chi} \left\{ \zeta_{i\chi}(\vec{\lambda}) \right\} > \zeta^{\max}. \end{cases} \tag{58}$$

Λ is the PIS (Λ_1 or Λ_2 for default), and $\zeta^{\max}$ is the design overrating boundary (1 for default). Note that the PIF can be calculated with the default PIS and rating to evaluate a topology in general, or with a custom PIS associated to a particular DES, to evaluate converters for a particular application. The $Z(\vec{\lambda})$ function depends on the converter.

The default MMC PIF is 0.1674 under dc compensation and 0.8837 under ac compensation. Both the PIF and the slices of the PIR show that the ac compensation mode is much more capable of achieving imbalances than the dc compensation mode, reaching 88.37% and 16.74% of the imbalance points respectively without requiring any overrating. The difference is quite significant, indicating that the operation mode should be a major factor to consider in the design of an MMC-DES.

VI. MODEL VALIDATION

The overrating model was validated through laboratory experiments with the setup depicted in Fig. 9 and the parameters of Table III. The experimental MMC-DES hardware is comprised by an MMC with dc power sources attached to the SM capacitors. The setup can operate in only two of the four identified modes (I and IV) because the power sources that emulate the DES are unidirectional. Nevertheless, those

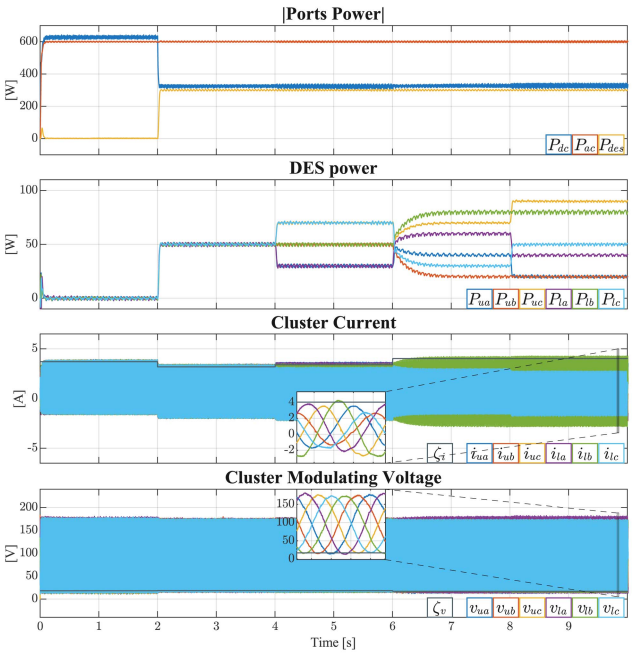

FIGURE 10. Mode I experiment.

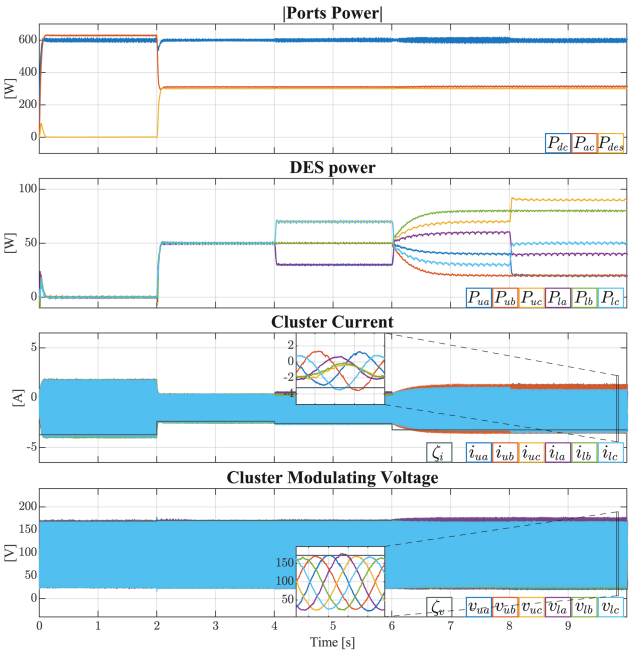

FIGURE 11. Mode IV experiment.

TABLE 4. Test Imbalance Sequence

Section	$\vec{\lambda^{\Sigma}}$	$\vec{\lambda^{\Delta}}$
1	$[0,0,0]^T$	$[0,0,0]^T$
2	$[0.5,0.5,0.5]^T$	$[0,0,0]^T$
3	$[0.3,0.5,0.7]^T$	$[0,0,0]^T$
4	$[0.5,0.5,0.5]^T$	$[0.1,0.3,-0.2]^T$
5	$[0.3,0.5,0.7]^T$	$[0.1,0.3,-0.2]^T$

TABLE 5. Overrating Model Evaluation Along Test Sequence in Experiments

Section	Error	Mode I	Mode IV
1	$\max\{\lvert i_{y\chi}\rvert\}$	−1.07%	−4.71%
	ζ_i	0%	0%
2	$\max\{\lvert i_{y\chi}\rvert\}$	−0.86%	−3.57%
	ζ_i	0.19%	0.76%
3	$\max\{\lvert i_{y\chi}\rvert\}$	−1.23%	−2.30%
	ζ_i	−0.15%	1.71%
4	$\max\{\lvert i_{y\chi}\rvert\}$	0.47%	−5.91%
	ζ_i	1.66%	−1.12%
5	$\max\{\lvert i_{y\chi}\rvert\}$	−0.22%	−5.82%
	ζ_i	0.92%	−1.02%

modes serve to evaluate both compensations. The remaining operating modes were evaluated using simulations of the experimental converter.

The experiments and simulations follow the imbalance reference sequence shown in Table IV. The chosen sequence goes through all possible kinds of imbalances individually, which allows to identify if there are particular weaknesses in the expressions. Also, using the same sequence for all modes allows to have a fair comparison between all the different operating modes.

The plots display the maximum predicted value of the currents and voltages. For the current, it is calculated as

$$\max_{y,\chi,t}\{|i_{y\chi}|\} = \max_{\chi}\left\{\zeta_{i\chi}\left(\vec{\lambda}_0^{\Sigma\Delta}\right)\right\}\cdot I_{y\chi}^{\text{nom}} \tag{59}$$

and it is calculated in a similar manner for the voltage.

The experimental results (see Figs. 10 and 11) are considered satisfactory. At first glance, they verify that the changes in converter voltage are not significant in relation to the nominal voltage, and that the cluster currents do change in a more noticeable degree. The model follows the changes in current magnitude correctly but with small imprecisions. The errors observed in the predicted overrating and maximum current are below 2% and 6%, respectively (see Table V).

The imprecisions can be tracked down to the first section of the test, where the model determines an inaccurate nominal current value, allegedly due to the lack of losses in the model. From there, it is not surprising to observe a slight current miscalculation in the subsequent test sections. With a good estimation of the nominal current, the maximum current error is much closer to the overrating error.

The simulations show that the currents of modes II and III behave similarly to the ones of modes I and IV, respectively, but with negated values (see Figs. 12 and 13). The model seems capable of estimating the maximum cluster currents with acceptable accuracy in these modes as well. Table VI presents the resulting current and overrating errors, which are always below 3%. Ultimately, these simulations allow to say that the model error varies within a narrow margin in all modes of operation.

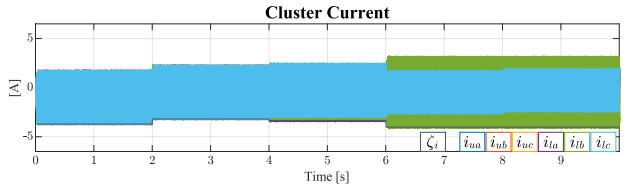

FIGURE 12. Mode II simulation.

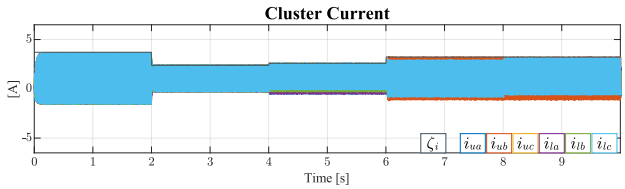

FIGURE 13. Mode III simulation.

TABLE 6. Overrating Model Evaluation Along Test Sequence in Simulations of Experimental Setup

Section	Error	Mode II	Mode III
1	$\max\{\lvert i_{y\chi}\rvert\}$	−0.54%	4.44%
	ζ_i	0%	0%
2	$\max\{\lvert i_{y\chi}\rvert\}$	−0.84%	2.60%
	ζ_i	−0.25%	−1.15%
3	$\max\{\lvert i_{y\chi}\rvert\}$	−0.65%	2.34%
	ζ_i	−0.10%	−1.43%
4	$\max\{\lvert i_{y\chi}\rvert\}$	−2.54%	2.84%
	ζ_i	−2.22%	−1.36%
5	$\max\{\lvert i_{y\chi}\rvert\}$	−2.48%	2.85%
	ζ_i	−2.15%	−1.35%

The Sections IV and V of the sequence were the ones that yielded the highest error in all modes of operation. These are the sections that have vertical imbalances, indicating that vertical imbalances are harder for the model to predict. Nevertheless, the error is still low. This phenomenon can be at least in part attributed to the discarding of the P^{Δ} loss terms during the derivation of the overrating expressions. Because the injection of compensatory currents (see Fig. 5) generates losses by interacting with the impedance of the cluster inductor (15).

So far, the two main sources of error identified in the model are the efficiency and the cluster inductor. Both of these issues should be less impactful in an industrial implementation, as i) a professional converter would be more efficient than the experimental setup; and ii) large scale MMC have smaller cluster inductors thanks to the higher number of levels and greater current magnitude, which results in smaller losses related to the compensatory currents.

To validate this hypothesis, simulations with parameters more akin to an industrial implementation were conducted (see Table VII). Fig. 14 displays the obtained current and prediction for one of the operating modes.

The obtained current and overrating estimation errors are below 2% and 1%, respectively, over all operating modes.

TABLE 7. Industrial Converter Simulation Parameters

Description	Parameter	Value
Nominal power	P^{nom}	1 MW
Dc grid voltage	V_{dc}	2 kV
Ac grid voltage	V_g	680 V
Cluster inductance	L_s	0.2 mH
Output inductance	L_o	0.1 mH
Cluster resistance	R_s	0.022 Ω
Output resistance	R_o	0.01 Ω
SM dc source voltage	V_{SM}	333.3 V
SMs per cluster	N	6
SM capacitance	C_{SM}	1 mF
SM switching frequency	f_{sw}	1.6 kHz

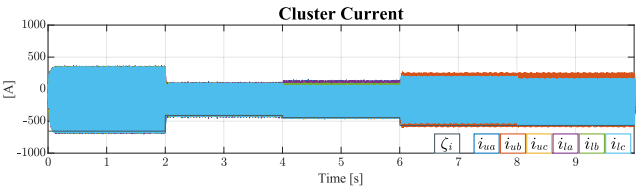

FIGURE 14. Mode IV industrial simulation.

This is less than what was observed in the experiments and the simulations of the experimental setup. This seems to confirm that losses are the main source of the small error observed in the model. And it indicates that the accuracy of the expressions would indeed improve in real implementations.

VII. CONCLUSION

This article introduces new metrics and a symbolic representation of the intercluster power imbalance magnitude of an MMC-DES, the imbalance factors λ_{χ}^{Σ} and λ_{χ}^{Δ}. It also derives overrating factors $\zeta_{i\chi}$ and $\zeta_{v\chi}$, establishing an analytical relation between imbalances and the resulting cluster overcurrent and overvoltage. This article utilized the derived expressions to thoroughly analyze the effects of imbalances in the converter operation, and the overall capacity for the converter to be unbalanced.

These new analytical expressions can be used in the design stage of the converter to rate the semiconductors and thermal system, based on the expected imbalances that the DES in question may achieve. Alternatively, they can be used to identify if a determined converter lacks the capacity to reach certain imbalance regions of a DES, and incorporate those limitations into the converter control.

Analysis shows that MMCs can be comfortably imbalanced in most scenarios if controlled under ac compensation. Therefore, it is far more convenient to incorporate variable DESs in applications that require or allow flexibility in the ac port of the MMC instead of the dc port. As most papers encompass only dc compensation, the consideration of ac compensation can make some existing proposals more appealing. Experiments and simulations successfully validate the formulated imbalance model and its subsequent analysis. They showed

that the efficiency of the converter affects the accuracy of the expressions.

Future work can use the developed expressions and metrics to conduct a detailed analytical comparison between the MMC-DES and CHB-DES, as there is a need to clarify the circumstances under which each converter can offer advantages against the other. In addition, more research is needed to study the performance of the converter across the different imbalance conditions and operating modes. Along with imbalances, there are other MMC-DES challenges that also require further research. Some of them are determining the appropriate SM topologies for each type of DES; fault detection, as typical MMC fault detection methods would need adjustments due to the change in topology; and control design to ensure a reliable integration of the MMC and the DES. In particular, the presented analysis can serve as a direct input for future reliability and failure analysis.

ANNEX A. SPECIAL SYMBOLOGY

VARIABLES AND PARAMETERS

$\Sigma\Delta$	Sigma-Delta transform.
λ	Imbalance factor.
ζ	Overrating factor.
κ	Power direction between MMC main ports, $\in \{-1, 1\}$
Γ	Custom function for overrating model compactness.
Λ	Bounded space of imbalance factors.
Z	Imbalance feasibility function.

SUBSCRIPTS

ϵ	Auxiliary term for compactness.
dc	Dc port.
ac	Ac port.
g	Ac grid.
des	DES attribute.
0	Dc frequency.
1	Ac fundamental frequency.
h	Frequency components, $h \in \{0, 1\}$
avg	Average value.
δ	Deviation from average value.
i	Current.
v	Voltage.

SUPERSCRIPTS

Σ	Σ component.
Δ	Δ component.
$\Sigma\Delta$	Set of Σ and Δ values.
$+, -, 0$	Sequence components.
p	Primary component.
c	Compensatory component.
nom	Nominal value.
dc	Dc compensation.
ac	Ac compensation.
max	Maximum value.

REFERENCES

[1] I. Trintis, S. Munk-Nielsen, and R. Teodorescu, "A new modular multilevel converter with integrated energy storage," in *Proc. 37th Annu. Conf. IEEE Ind. Electron. Soc.*, 2011, pp. 1075–1080, doi: 10.1109/IECON.2011.6119457.

[2] M. Vasiladiotis and A. Rufer, "Analysis and control of modular multilevel converters with integrated battery energy storage," *IEEE Trans. Power Electron.*, vol. 30, no. 1, pp. 163–175, Jan. 2015, doi: 10.1109/TPEL.2014.2303297.

[3] Q. Chen, R. Li, and X. Cai, "Analysis and fault control of hybrid modular multilevel converter with integrated battery energy storage system," *IEEE Trans. Emerg. Sel. Topics Power Electron.*, vol. 5, no. 1, pp. 64–78, Mar. 2017, doi: 10.1109/JESTPE.2016.2623672.

[4] F. Gao, L. Zhang, Q. Zhou, M. Chen, T. Xu, and S. Hu, "State-of-charge balancing control strategy of battery energy storage system based on modular multilevel converter," in *Proc. IEEE Energy Convers. Congr. Expo.*, 2014, pp. 2567–2574, doi: 10.1109/ECCE.2014.6953744.

[5] T. Soong and P. W. Lehn, "Assessment of fault tolerance in modular multilevel converters with integrated energy storage," *IEEE Trans. Power Electron.*, vol. 31, no. 6, pp. 4085–4095, Jun. 2016, doi 10.1109/TPEL.2015.2477834.

[6] T. Soong and P. W. Lehn, "Evaluation of emerging modular multilevel converters for bess applications," *IEEE Trans. Power Del.*, vol. 29, no. 5, pp. 2086–2094, Oct. 2014, doi: 10.1109/TPWRD.2014.2341181.

[7] P. D. Judge and T. C. Green, "Modular multilevel converter with partially rated integrated energy storage suitable for frequency support and ancillary service provision," *IEEE Trans. Power Del.*, vol. 34, no. 1, pp. 208–219, Feb. 2019, doi: 10.1109/TPWRD.2018.2874209.

[8] G. Wang et al., "A review of power electronics for grid connection of utility-scale battery energy storage systems," *IEEE Trans. Sustain. Energy*, vol. 7, no. 4, pp. 1778–1790, Oct. 2016, doi: 10.1109/TSTE.2016.2586941.

[9] Z. Blatsi, P. D. Judge, S. J. Finney, and M. M. C. Merlin, "Blackstart capability of modular multilevel converters from partially-rated integrated energy storage," *IEEE Trans. Power Del.*, vol. 38, no. 1, pp. 268–276, Feb. 2023, doi: 10.1109/TPWRD.2022.3188907.

[10] S. Ali, Z. Ling, K. Tian, and Z. Huang, "Recent advancements in submodule topologies and applications of MMC," *IEEE Trans. Emerg. Sel. Topics Power Electron.*, vol. 9, no. 3, pp. 3407–3435, Jun. 2021, doi: 10.1109/JESTPE.2020.2990689.

[11] A. F. Cupertino, W. C. S. Amorim, H. A. Pereira, S. I. Seleme Junior, S. K. Chaudhary, and R. Teodorescu, "High performance simulation models for ES-STATCOM based on modular multilevel converters," *IEEE Trans. Energy Convers.*, vol. 35, no. 1, pp. 474–483, Mar. 2020, doi: 10.1109/TEC.2020.2967314.

[12] S. K. Chaudhary, A. F. Cupertino, R. Teodorescu, and J. R. Svensson, "Benchmarking of modular multilevel converter topologies for es-statcom realization," *Energies*, vol. 13, no. 13, 2020, Art. no. 3384, doi: 10.3390/en13133384.

[13] B. Novakovic and A. Nasiri, "Modular multilevel converter for wind energy storage applications," *IEEE Trans. Ind. Electron.*, vol. 64, no. 11, pp. 8867–8876, Nov. 2017, doi: 10.1109/TIE.2017.2677314.

[14] M. Quraan, T. Yeo, and P. Tricoli, "Design and control of modular multilevel converters for battery electric vehicles," *IEEE Trans. Power Electron.*, vol. 31, no. 1, pp. 507–517, Jan. 2016, doi: 10.1109/TPEL.2015.2408435.

[15] D. Ronanki and S. S. Williamson, "Modular multilevel converters for transportation electrification: Challenges and opportunities," *IEEE Trans. Transport. Electrific.*, vol. 4, no. 2, pp. 399–407, Jun. 2018, doi: 10.1109/TTE.2018.2792330.

[16] M. Quraan, P. Tricoli, S. D'Arco, and L. Piegari, "Efficiency assessment of modular multilevel converters for battery electric vehicles," *IEEE Trans. Power Electron.*, vol. 32, no. 3, pp. 2041–2051, Mar. 2017, doi: 10.1109/TPEL.2016.2557579.

[17] S. Rivera, B. Wu, R. Lizana, S. Kouro, M. Perez, and J. Rodriguez, "Modular multilevel converter for large-scale multistring photovoltaic energy conversion system," in *Proc. IEEE Energy Convers. Congr. Expo.*, 2013, pp. 1941–1946, doi: 10.1109/ECCE.2013.6646945.

[18] A. B. Acharya, M. Ricco, D. Sera, R. Teodorescu, and L. E. Norum, "Arm power control of the modular multilevel converter in photovoltaic applications," *Energies*, vol. 12, no. 9, 2019, Art. no. 1620, doi: 10.3390/en12091620.

[19] J. Zhou et al., "Design and control of power fluctuation delivery for cell capacitance optimization in multiport modular solid-state transformers," *IEEE Trans. Power Electron.*, vol. 36, no. 2, pp. 1412–1427, Feb. 2021, doi: 10.1109/TPEL.2020.3006956.
[20] A. Shojaei and G. Joós, "A topology for three-stage solid state transformer," in *Proc. IEEE Power Energy Soc. Gen. Meeting*, 2013, pp. 1–5, doi: 10.1109/PESMG.2013.6672781.
[21] F. Briz, M. Lopez, A. Rodriguez, and M. Arias, "Modular power electronic transformers: Modular multilevel converter versus cascaded H-bridge solutions," *IEEE Ind. Electron. Mag.*, vol. 10, no. 4, pp. 6–19, Dec. 2016, doi: 10.1109/MIE.2016.2611648.
[22] D. Li, Z. Ji, Y. Sun, J. Zhao, and C. Zhang, "Four-port solid-state transformer based on hybrid MMC with enhanced dual half-bridge submodules," *IET Power Electron.*, vol. 13, no. 12, pp. 2432–2441, 2020, doi: 10.1049/iet-pel.2019.1304.
[23] M. A. Perez, D. Arancibia, S. Kouro, and J. Rodriguez, "Modular multilevel converter with integrated storage for solar photovoltaic applications," in *Proc. 39th Annu. Conf. IEEE Ind. Electron. Soc.*, 2013, pp. 6993–6998, doi: 10.1109/IECON.2013.6700292.
[24] M. Schroeder and J. Jaeger, "Advanced energy flow control concept of an MMC for unrestricted operation as a multiport device," *IEEE Trans. Power Electron.*, vol. 34, no. 11, pp. 11496–11512, Nov. 2019, doi: 10.1109/TPEL.2019.2902098.
[25] A. Dekka, B. Wu, R. L. Fuentes, M. Perez, and N. R. Zargari, "Evolution of topologies, modeling, control schemes, and applications of modular multilevel converters," *IEEE Trans. Emerg. Sel. Topics Power Electron.*, vol. 5, no. 4, pp. 1631–1656, Dec. 2017, doi: 10.1109/JESTPE.2017.2742938.
[26] M. A. Perez, S. Bernet, J. Rodriguez, S. Kouro, and R. Lizana, "Circuit topologies, modeling, control schemes, and applications of modular multilevel converters," *IEEE Trans. Power Electron.*, vol. 30, no. 1, pp. 4–17, Jun. 2015, doi: 10.1109/TPEL.2014.2310127.
[27] G. Liang et al., "Analytical derivation of intersubmodule active power disparity limits in modular multilevel converter-based battery energy storage systems," *IEEE Trans. Power Electron.*, vol. 36, no. 3, pp. 2864–2874, Mar. 2021, doi: 10.1109/TPEL.2020.3014739.
[28] R. Darus, J. Pou, G. Konstantinou, S. Ceballos, and V. G. Agelidis, "A modified voltage balancing sorting algorithm for the modular multilevel converter: Evaluation for staircase and phase-disposition PWM," in *Proc. IEEE Appl. Power Electron. Conf. Expo.*, 2014, pp. 255–260, doi: 10.1109/APEC.2014.6803318.
[29] L. Zhang, Y. Tang, S. Yang, and F. Gao, "Decoupled power control for a modular-multilevel-converter-based hybrid ac-dc grid integrated with hybrid energy storage," *IEEE Trans. Ind. Electron.*, vol. 66, no. 4, pp. 2926–2934, Apr. 2019, doi: 10.1109/TIE.2018.2842795.
[30] P. Munch, D. Gorges, M. Izák, and S. Liu, "Integrated current control, energy control and energy balancing of modular multilevel converters," in *Proc. 36th Annu. Conf. IEEE Ind. Electron. Soc.*, 2010, pp. 150–155, doi: 10.1109/IECON.2010.5675185.
[31] T. Soong and P. W. Lehn, "Internal power flow of a modular multilevel converter with distributed energy resources," *IEEE Trans. Emerg. Sel. Topics Power Electron.*, vol. 2, no. 4, pp. 1127–1138, Dec. 2014, doi: 10.1109/JESTPE.2014.2342656.
[32] Y. Yu, G. Konstantinou, B. Hredzak, and V. G. Agelidis, "Power balance optimization of cascaded H-bridge multilevel converters for large-scale photovoltaic integration," *IEEE Trans. Power Electron.*, vol. 31, no. 2, pp. 1108–1120, Feb. 2016, doi 10.1109/TPEL.2015.2407884.
[33] Y. Yu, G. Konstantinou, C. D. Townsend, R. P. Aguilera, and V. G. Agelidis, "Delta-connected cascaded H-bridge multilevel converters for large-scale photovoltaic grid integration," *IEEE Trans. Ind. Electron.*, vol. 64, no. 11, pp. 8877–8886, Nov. 2017, doi 10.1109/TIE.2016.2645885.
[34] G. Liang et al., "Unbalanced active power distribution of cascaded multilevel converter-based battery energy storage systems," *IEEE Trans. Ind. Electron.*, vol. 69, no. 12, pp. 13022–13032, Dec. 2022, doi: 10.1109/TIE.2021.3137442.
[35] Y. Pan, X. Sun, W. Zhao, X. Li, and Y. Cai, "Research on limits of uneven battery power in modular multilevel converter-based battery energy storage system," *CSEE J. Power Energy Syst.*, early access, Sep. 5, 2022, doi: 10.17775/CSEEJPES.2021.01510.
[36] M. Hagiwara and H. Akagi, "Control and experiment of pulsewidth-modulated modular multilevel converters," *IEEE Trans. Power Electron.*, vol. 24, no. 7, pp. 1737–1746, Jul. 2009, doi: 10.1109/TPEL.2009.2014236.
[37] A. Antonopoulos, L. Angquist, and H.-P. Nee, "On dynamics and voltage control of the modular multilevel converter," in *Proc. 13th Eur. Conf. Power Electron. Appl.*, 2009, pp. 1–10.

TOMAS SALVADORES (Student Member, IEEE) received the B.Sc. and M.Sc. degrees in electrical engineering from Pontificia Universidad Católica de Chile, Santiago, Chile, in 2021 and 2023, respectively.

Since 2023, he has been a Development Engineer with Muon Vision Inc. His research interests include design requirements and control algorithms for battery energy storage integration in modular multilevel converters, renewable energy, use of neural networks for power converter control, and muon radiography.

JAVIER PEREDA (Senior Member, IEEE) received the B.Sc. (Eng.) degree with highest honors in electrical engineering, in 2009, and the M.Sc. and Ph.D. degrees in electrical engineering, in 2013, all from Pontificia Universidad Católica de Chile, Santiago, Chile.

In 2013, he joined the Electrical Department, Pontificia Universidad Católica de Chile, where he is currently an Associate Professor. From 2014 to 2016, he was an Associate Research with the Control and Power Group, Department of Electrical and Electronic Engineering, Imperial College London, U.K. He is an Associate Research of the UC Energy Research Center, Chile, and the Solar Energy Research Center (SERC Chile). He is the Principal Investigator of the Electric Vehicle Laboratory and the Power and Energy Conversion Laboratory (PEClab), Pontificia Universidad Católica de Chile. His research interests include power electronics and control applied to electric vehicles, energy storage, ac and dc electric networks, renewable energy, multilevel converters, industrial applications, and motor drives.

FÉLIX ROJAS (Member, IEEE) was born in Santiago, Chile. He received the B.Eng. and M.Sc. degrees in electrical engineering (hons.) from the Universidad de Santiago de Chile, Santiago, Chile, in 2009, and the doctoral degree in electrical engineering from the Technical University of Munich, Munich, Germany, in 2016.

He is currently an Associate Professor with Electrical Department, Pontificia Universidad Catolica de Chile, Santiago, Chile, and the Principal Investigator of the Electric Vehicle Laboratory and the Power and Energy Conversion Laboratory (PEClab), Pontificia Universidad Catolica de Chile. He is also Associate Research with the Solar Energy Research Center (SERC Chile) and the UC Energy Research Center, Santiago, Chile. From 2016 to 2021, he was Associate Professor of electrical engineering with the University of Santiago, Santiago, Chile, and the Head of Electrical Energy Technologies Research Center (E2TECH), University of Santiago, Santiago, Chile. His research interests include the control of modular multilevel converters, solid state transformers, renewable energy conversion, electric vehicles chargers, and machine drives.